Synthesis And Characterization of Cobalt-Zinc Spinel Ferrites For High Frequency Applications

Salma Aman
Khwaja Fareed University of Engineering & Information Technology
Tahani I. Al-Muhimeed
King Saud University
Zaki Ismail Zaki
Taif University
Zeinhom M. El-Bahy
Al-Azhar University
Abeer A. AlObaid
King Saud University
H.H. Hegazy
King Khalid University
Rabia Yasmin Khosa
University of Education
Adeela Rehman
Kyung Hee University
Syeda Rabia Ejaz
The Government Sadiq College Women University Bahawalpur
Hafiz Muhammad Tahir Farid (tahirfaridbzu@gmail.com)
Bahauddin Zakariya University https://orcid.org/0000-0002-4232-7939

Research Article

Keywords: XRD, High Frequency Applications, Resistivity, Magnetic materials, Dielectric loss

Posted Date: September 15th, 2021

DOI: https://doi.org/10.21203/rs.3.rs-861279/v1

Abstract

Spinel ferrites are attractive for high frequency applications due to their larger direct current (dc) resistivity and low dielectric loss. In the present work, $Co_{0.6}Zn_{0.4}Ho_xFe_{2-x}O_4$ (x = 0.00 and 0.1) spinel ferrites were prepared by sol-gel method. The X-ray diffraction pattern showed that both samples had cubic spinel structure, while in sample (x = 0.1), the secondary phase ($HoFeO_3$) was also observed. The dc resistivity was increased with the addition of holmium ions. As the temperature increased, the dc resistivity was decreased by proving their semiconducting nature. The dielectric properties were also measured as a function of temperature and frequency. The sample which was composed by the substitution of holmium ions contained low value of dielectric loss. The magnetic properties were also experimentally measured by applying the field up to 2000 oersted. The small area covered by hysteresis loop proved that both samples possessed soft nature of magnetic materials.

Introduction

Currently, the researchers are investigating the materials that can be functioned properly in microwave absorption band and utilized as electromagnetic absorbents [1–2]. Such kind of materials is comprehensively used in electronic and communication devices. They have plenty of applications in scientific, industrial, military, and commercial areas, which include radar exposure techniques, wireless network systems, mobile phones, and computers. These materials are utilized as metallic surfaces in the shielding of extremely reflective surfaces by decreasing the radar cross-section of the targets and removing the issue of electromagnetic compatibility (EMC) and electromagnetic interference (EMI) [3–5]. When the incoming microwave, which is actually a pairing of vibrating electric field and magnetic field, strikes upon the material's surface, the particles of material interact with either one field or both fields in order to derive the matter/light interactions under the GHz frequency section of EM spectrum [6]. The interactions with both or any of the fields follow Maxwell's relations. According to Maxwell's relations, the interactions of material particles with any field will produce the response of others. Consequently, the whole EM wave dissipated [7]. Moreover, the energy engrossed by the material is the energy of the EM wave, which is then converted into thermal energy because of the magnetic and dielectric response of the material. Nowadays, ferrite nanoparticles are supposed to be talented candidates for EM wave absorbers under higher frequency ranges due to their larger values of saturation magnetization and high Snoek's limit and, consequently, greater permeability figures at the gigahertz range [8]. Ferrites are considered magnetic substances with EM radiation-absorbing capabilities via hysteresis loss mechanism, domain wall resonance, and eddy current effect [9]. The particular type of ferrites is named spinel ferrite having the molecular formula $MeFe_2O_4$. Here, "Me" is divalent metallic ion such as Mg^{2+}, Mn^{2+}, Co^{2+}, Ni^{2+}, Cu^{2+}, Zn^{2+}, Cd^{2+}etc. Among spinel ferrites, the cobalt zinc ferrites have several useful features. Cobalt zinc ferrites are important components of microwave devices such as isolators, circulars, gyrators, phase shifters, and memory cores due to their high Curie temperature, high saturation magnetization, and hysteresis loop properties, which offer a performance advantage over other spinel structures [10]. The well-known Co-Zn category of ferrites is soft magnetic materials with numerous high-frequency

instruments like electromagnetic interference filters and multilayer chip inductors. They have many valuable features such as chemical stability, fewer loss values at higher frequency areas, permeability, resistivity, magnetization, Curie temperature [11]. The substituent ions can occupy different lattice sites, they can alter the structural, electromagnetic, and other physical properties of host matter based on their site preferences [12]. As a result, magnetic fields can control electrical properties. This has rekindled the desire to discover new methods of improving the properties and expectations of these materials in practical applications. The spin connection of 3d electrons causes ferroelectric and ferromagnetic properties during Fe-Fe interactions. Rare earth ions (which belong to the 4f elements) partially substitute for the Fe^{3+} ions in spinel ferrites, resulting in 3d-4f coupling. As a result, electrons with ferroelectric and ferromagnetic properties [13] are used in spinel ferrites. The addition of rare earth metal ions, such as holmium, alters the structural and textured properties of the material. Rare Earth oxides, which are excellent electric isolators, have a resistivity of about 10^8 Ω-cm. These ions occupy B sites, which obstruct the movement of Fe^{2+} during the ferrite conduction process, increasing the compound's electrical resistivity. Holmium is an excellent dopant for all other lanthanides due to its excellent thermal and ferroelectric properties. By reducing the particle size of the host compound, incorporation of holmium ions into the spinal cord can increase electric resistance and decrease saturation magnetization [14, 15].

In the present study, the Sol-gel method gave a homogeneous mixture of materials. This method can be adopted due to its low cost. The preparation of each sample by the sol-gel method takes lesser time as compared to other methods. So, we used the sol-gel technique to prepare this ferrite system. In the sol-gel technique, the samples can be synthesized at a relatively lesser temperature [16]. The Co-Zn-ferrites have advantageous features like high resistivity and low dielectric losses. In current inspection, manufactured systems' electrical and dielectric properties are evaluated under a wide temperature range as a function of frequency.

Experimental Details

For preparing the samples, all metal nitrates were taken, cobalt nitrate [$Co(NO_3)_2$ (Daujung 99.90 %)], zinc nitrate [$Zn(NO_3)_2.6H_2O$ (unit-chem 99.90 %)], Holmium nitrate [$Ho(NO_3)_3$] and iron nitrate [$Fe(NO_3)_3.9H_2O$ (sigma Aldrich 99.90 %)]. The citric acid monohydrate (Merck 99.9%) $C_6H_6O_7.H_2O$ acted like a chelating agent. They were further taken with no impurity. The solution molarity value is chosen at 0.01mole. Along with that molarity the appropriate values were chosen for the nitrates. The liquefaction of every nitrate was done distinctly in hundred Milli litter of de-ionized water. A distinct solution of the citric acid is synthesized in the 100 Milli-litter of H_2O. The amount of the citric acid has taken according with the valences of metal ions. For all-nitrates the solutions were prepared individually, also stirred well enough in a hot plate about ten minutes. Then the mixing and stirring continuously had done on a hot plate. The stirring process was continued at 80 degree centigrade. The pH of solution was kept at 7 by the addition of ammonia during stirring. After 5 to 6 hour the solution become like a viscous gel. Then whole prepared material was placed in an oven for six hours at temperature 523 K. This gel then turned into the blackish brittle flake. Agate Mortar and pestle were used to achieve the wet blending of chemicals from the mixture

of raw chemicals with deionized water. The product is made homogeneous by drying procedure and calcinated at 800 ^{o}C for three hours. The product is cooled under normal temperature conditions. A small quantity of polyvinyl alcohol is mixed as the binder. The product is ready for grinding. After completing the grinding process, the uniaxial pellets are prepared using stainless steel die under the pressure of 3–8 ton/in2. The sintering process of pellets is completed under 1000 ^{o}C temperature and again cooled at room temperature slowly. The prepared spinel ferrites have no required phase at low temperatures (600 ^{o}C). By studying different research papers, all the samples were sintered at high temperatures (1000 ^{o}C) and got the required results [17, 18].

The structural analysis was done using an X-ray diffractometer having CuKα as a radiation source (λ = 1.54 Å). Before the electrical and dielectric analysis, the surface of pellets is sprayed with silver paste, making the contacts better. The dielectric study was completed through an LCR meter made up of Agilent Technologies. The measurements are analyzed in the 0.075 to 20 MHz frequency range. The Keithley instrument was used to study electrical behavior under the temperature range of 293 to 473 K.

Results And Discussion

The cubic spinel structure of prepared samples was estimated from the X-ray diffraction (XRD) details presented in Fig. 1. Sharp peaks were seen in XRD data. The XRD peaks for samples having composition x = 0.1 are wider with smaller intensity values. The diffraction planes (111), (220), (222), (311), (400), (422), (333), and (440) showed the cubic spinel structure of prepared samples. All these peaks were well-matched with standard JCPDS card (88-1942). All the samples possessed a simple cubic structure and were categorized in the Fd-3m space group. No secondary phases were seen in the XRD pattern. The formula for the measurements of lattice constant is given as [18];

$$a = d_{hkl}\sqrt{h^2 + k^2 + l^2} \quad (1)$$

In Eq. (1), the h k l are miller indices and d is inner planer spacing. Various numerical values for lattice constant, ionic radii, jump lengths as well as bond lengths of tetrahedral and octahedral sites were displayed in Table 1. The greater value of lattice constant for x = 0.1 sample is due to bigger size of Ho^{3+} as compared to Fe^{3+}. These results are well matched with previous presented paper results [19, 20].

Table 1
Different structural parameters of spinel ferrites.

Concentration	a [Å]	r_A [Å]	r_B [Å]	A-O [Å]	B-O [Å]	L_A [Å]	L_B [Å]	Room Temperature Resistivity [Ω-cm]
x = 0.00	8.310	0.449	0.727	1.799	2.077	3.598	2.938	7.07×10^7
x = 0.1	8.334	0.453	0.732	1.803	2.082	3.607	2.945	2.63×10^8

The inner atomic vibrations were estimated from Fourier-transform infrared spectroscopy (FTIR) spectra. The structural behavior of samples is dependent upon the lattice vibrations. These vibrations vary with bonding force and mass of cations. The IR spectrum for both samples was shown in the Fig. 2. The absorption peaks of manufactured system under room temperature were positioned at 435 and 581. The existence of basic two absorption bands confirmed the successful formation of ferrites [21]. Two major bands parallel to stretching vibrations of A and B sites positioned between 600cm^{-1} and 400cm^{-1}[22]. The specific band at 581 cm^{-1} and 582cm^{-1} allotted to tetrahedral category complexes whereas the absorption bands at 435 accredited to tetrahedral category complexes [23].

The scanning electron microscopy (SEM) images for two samples were given in the Fig. 3. The nanoparticles are agglomerated and have spherical shape as seem in SEM micrographs. The inhomogeneous mixture can be seemed clearly from images. Similar facts were also reported in previous researches by some other authors [24, 25]. Two samples are selected for transmission electron microscopy (TEM) analysis. The TEM images were presented in the Fig. 4. TEM images showed that the particles have spherical shape and they formed clumps. The TEM data have good accordance with XRD data.

Table 1 shows the DC electrical resistivity at room temperature of $Co_{0.6}Zn_{0.4}Ho_xFe_{2-x}O_4$ (x = 0.0 and x = 0.1) spinel ferrites. Co-Zn ferrite is extremely resistant in spinel ferrites and has high activation energy. The methods for synthesizing doped cations at sites A and B, particulate size or morphology, as well as sintering conditions affect all of spinel ferrite's electro-power properties [26]. The DC electro-resistivity, as shown in Table 1, increases with the Ho^{3+} concentration. When Ho^{3+} (x = 0.1) is replaced, the electrical DC resistivity increases considerably. Due to electron hopping between Fe^{2+} and Fe^{3+}, the Verwey mechanism could easily explain the electrical conduction of spinel ferrites. The replacement of Ho^{3+} with octahedral ions (B location) decreases the number of Fe^{3+} ions on B sites, along with the $Fe^{3+}\leftrightarrow Fe^{2+}$ trend, reduces the conductivity and increases the resistivity.

The graph of DC resistivity for temperature was given in Fig. 5. From this figure, it is cleared that the resistivity was reduced with the surge of temperature. The reason for the high resistivity value is the presence of Ho^{3+}ion in the Co-Zn system. The quantity of Fe-ions reduced at the octahedral site due to Ho^{3+} substitution, which plays a central role in the conduction mechanism [26]. The DC resistivity value of pure Co-Zn-ferrites declined with the increase of temperature, obeying the eminent Arrhenius equation [27]. Thus, the Co-Zn system has semiconducting nature. More conduction electrons were originated with the upsurge of temperature, which in turn reduced the resistivity. The reduction in the resistivity with the activation of drift electrons followed the hopping conduction mechanism. The decrease of resistivity with the increase of temperature does not link the charge carrier's production. The conduction mechanism is mainly completed by the electrons hopping between ferric and ferrous ions, i.e., $Fe^{2+} \leftrightarrow Fe^{3+} + e^{-1}$.

The slope of the graph presented in Fig. 6 gives the value of activation energy. Usually, the activation energy of nano-ferrites depends upon the charge carrier's mobility. It is independent of the concentration

of charge carriers. Charge carriers merely stay at vacant positions. The hopping process completes the conduction procedure. The hopping procedure is determined by activation energy associated with the electrical barrier experienced by the electrons during the procedure [24]. Figure 7 contains different dielectric constant values for frequency ranges from 0.1MHz to 20MHz under fixed temperatures. Up to 1MHz frequency, the dielectric constant value slowly decreases and then becomes constant at 6MHz. Beyond this limit, its value increases. The reduction of dielectric constant below a particular frequency can be demonstrated on dipole relaxation occurrence [25, 26]. The increase of dielectric constant beyond the specific limit can be explained on behalf of the resonance phenomenon at high frequency. The resonance happened when the applied field frequency matched with the charge exchanging frequency $Fe^{3+} \leftrightarrow Fe^{2+}$. Wagner polarization model as well Maxwell theory, was used to clarify such type variations [27, 28].

The variation of dielectric constant for different temperature values under fixed frequency range was given in Fig. 8. For each value of frequency, the rise of temperature leads to an increase in the dielectric constant. The declined in dielectric constant was observed by substitution of the Holmium concentration. In decrease was observed through the ions substituted of the Holmium content also be clarified by the similar trend by the conduction technique of the electronic conduction. Here, the inter-conversion of electrons among Fe^{3+} and Fe^{2+} ions developed the displacement among charges increases, which supports finding out polarization of the charges through such ferrites. Therefore, the plenty of these Fe^{2+} ions at the octahedral site shows a competent role in the polarization of dielectric. Because of the greater ionic radius, the ions of Ho^{3+} take an octahedral site. Substitution of the Holmium ions for the ions of iron (site-B) blocks the mechanism of conduction because of its valence stability. It's purposed that the transfer of electrons could not take between the Ho^{3+} and Fe^{2+} ions. Thus, a decrease in dielectric polarization is observed. However, the increase in temperature is faster in lesser frequency areas and slowed down in higher frequency areas. Usually, the dielectric constant is related directly to dielectric polarization. There are four main kinds of polarizations: electronic polarization, ionic polarization, dipolar polarization, and space charge polarization. The dipolar and space charge polarization plays a central role in the lower frequency section, and they are temperature-dependent [29].

The dielectric loss versus temperature values under the specified range of frequency was displayed in Fig. 9. The dielectric loss reduced with the rise of frequency. This variation trend is due to resonance and follows Koop's Model [30, 31]. The phenomenon of resonance occurred when the hopping frequency matched with the applied field frequency. The data relating to the conduction process presented by Hudson explains the dielectric losses in ferrites. The substances with more excellent conductivity would have high loss values. The dielectric losses versus several frequency values under specified temperature were shown in Fig. 10. The trend of variation of dielectric loss is similar to the trend of dielectric constant and explained similarly. The results showed that the involvement of Ho^{3+} ions in Co-Zn -ferrites increased DC resistivity and decreased dielectric constant and dielectric loss. These changes are demonstrated by using the concept of the hopping mechanism ($Fe^{2+} \leftrightarrow Fe^{3+} + e^{-1}$). The substituted ion ($Ho^{3+}$) does not take part in the conduction mechanism. These ions only bound the hopping by stopping the $Fe^{2+} \leftrightarrow Fe^{3+}$

+ e^{-1} exchange on the octahedral site [32]. The quantity of Fe-ion lessened with the substitution of Ho^{3+}ion [33].

The measurements of magnetic factors were completed under the applied field of 2 kOe. Fundamentally that was ferromagnetic phenomenal. In the given magnetic field, we observed the explicit behavior of hysterics. Narrow loops indicate the soft type of such spinel ferrites. Moreover, we used the hysteresis loop to count the various magnetic parameters such as remanence (Mr), magnetization (Ms), and coercivity (Hc). The calculation of saturation magnetization is done with magnetization curve on the Hmax also observes a falling trend by raising the Holmium contents. We observed the behavior of soft magnetic through thin M-H loop because of their fewer coercivity values. The ferromagnetic nature was confirmed from the characterization results as given in Fig. 11. The coercivity value enlarged while the saturation magnetization dropped. The replacement of Ho^{3+} ions with Fe^{3+} ions reduced the quantity of Fe^{3+} ions at the octahedral site. The magnetic moment value of RE ion is significantly less than Fe-ion [32, 33]. Consequently, the magnetization values dropped.

The loss in flagging off the AB-exchange interfaces was the only cause of the loss in saturation magnetization and the remanence. The three types of negative exchange interactions occurred among both ions of those electrons that were unpaired on sites B and A. Among these three interactions, the interaction A-B predominates upon the remaining two, for example, interaction B-B and A-A. For the spinel ferrites given, we considered Ho^{3+} ions such as minimum magnetic substance value on the room temperature also attain to the sites-B(an octahedral site). In contrast, the ions of Fe^{3+} are occupied with both sites B as well as A. Like in the spinel ferrite, the total magnetic moments relay at the no. of the magnetic ions attaining to the octahedral (B) and tetrahedral (A) sites; create the saturation magnetization decreasing value. The Ho ions substitution (1.00 Å ionic radius) on the ions of Fe^{3+} (0.64 Å ionic radius) occurred on the octahedral sites also its existence on the sites of tetrahedral is founded very rare. Hence, the reduction of the octahedral site in the number of magnetic moments is expected. Thus we observed a reduction in the magnetic moment on lattice-B that consequently causes to decreases the magnetization, and eventually, in net magnetization, we observed a decrease. In the current study, by substituting Holmium, the reduction in magnetization is the best deal by the previously described work of many more researchers.

Conclusion

- The sol-gel method was adopted to achieve Ho substituted Co-Zn-ferrites.
- All the samples possessed a simple cubic structure.
- The DC resistivity value was enhanced up to 2.63×10^8 Ω-cm with Ho^{3+} ion substitution. The compounds with high DC resistivity are appropriate for higher frequency applications.
- The decrease of resistivity with higher temperature showed the semiconducting nature of samples.
- At room temperature and 20MHz frequency, the dielectric was found to be 1.4.

- Lesser values of dielectric loss and larger value of resistivity suggested that the sample (x = 0.10) may be suitable for high frequency applications.

Declarations

Acknowledgement

This work was financially supported by the Taif Researchers Supporting Project (TURSP-2020/42), Taif University, Taif, Saudi Arabia.The authors extend their appreciation to the Researchers Supporting Project number (RSP-2021/381), King Saud University, Riyadh, Saudi Arabia. The author (H.H. Hegazy) extends his appreciation to the Deanship of Scientific Research at King Khalid University for the financial support through research groups program under grant number (G.R.P/199/42).

References

1. Farid HMuhammadT, Ahmad I, Ali I, Ramay SM, Mahmood A (2019) Study of spinel ferrites with addition of small amount of metallic elements. J Electroceram 42:57
2. Kanwal M, Ahmad I, Meydan T, Cuenca JA, Williams PI, Farid MT, Murtaza G (2018) Structural, Magnetic and Microwave Properties of Gadolinium-Substituted Ca-Ba M-Type Hexagonal Ferrites. Journal of Electronic Materials Volume 47(9):5370–5377
3. Wu F, Sun H, AJia IA, Roqan IS, Zhang D, Dai J, Chen C, Feng ZC, Li X, Significant internal quantum efficiency enhancement of GaN/AlGaN multiple quantum wells emitting at ~ 350 nm via step quantum well structure design, Journal of Physics D: Applied Physics 50 (24), 245101
4. Shabana Munir I, Ahmad A, Laref (2020) Muhammad Tahir Farid, Effect of Nd-Substitution on Hexagonal Ferrites for Memory Devices. Journal of Applied Physics A-Materials Science Processing 126:722
5. Ashiq MN, Naz F, Malana MA, Gohar RS, Ahmad Z (2012) Role of Co–Cr substitution on the structural, electrical and magnetic properties of nickel nano-ferrites synthesized by the chemical co-precipitation method. Mater Res Bull 47:683–686
6. Aravindh SA, Schwingenschloegl U, Roqan IS, Ferromagnetism in Gd doped ZnO nanowires: a first principles study, Journal of Applied Physics 116 (23), 233906
7. Ajia IA, Edwards PR, Pak Y, Belekov E, Roldan MA, Wei N, Liu Z, Generated carrier dynamics in V-pit-enhanced InGaN/GaN light-emitting diode, ACS Photonics 5 (3), 820–826
8. Alfaraj N, Mitra S, Wu F, Ajia IA, Janjua B, Prabaswara A, Aljefri RA, Sun H, Photoinduced entropy of InGaN/GaN pin double-heterostructure nanowires Applied Physics Letters 110 (16), 161110
9. Muhammed MM, Alwadai N, Lopatin S, Kuramata A, Roqan IS, High-Efficiency InGaN/GaN Quantum Well-Based Vertical Light-Emitting Diodes Fabricated on β-Ga2O3 Substrate, ACS applied materials & interfaces 9 (39), 34057–34063

10. Flemban TH, Sequeira MC, Zhang Z, Venkatesh S, Alves E, Lorenz K, Identifying the influence of the intrinsic defects in Gd-doped ZnO thin-films, Journal of Applied Physics 119 (6), 065301
11. Zhang Z, Schwingenschlögl U, Roqan IS, Possible mechanism for d 0 ferromagnetism mediated by intrinsic defects, RSC Advances 4 (92), 50759–50764
12. Kumar N, Singh RK, Satyapal HK (2020) Structural, optical, and magnetic properties of non-stoichiometric lithium substituted magnesium ferrite nanoparticles for multifunctional applications. J Mater Sci: Mater Electron 31:9231–9241
13. Aravindh SDA, Schwingenschloegl U, Roqan IS, Defect induced d0 ferromagnetism in a ZnO grain boundary, The Journal of chemical physics 143 (22), 224703
14. Farid HMuhammadT, Ahmad I, Ali I, Ramay SM, Mahmood A, Murtaza G (2017) Dielectric and impedance study of praseodymium substituted Mg-based spinel ferrites. J Magn Magn Mater 434:143–150
15. Dong Limin H, Zhidong Z, Yaoming Wu, Ze Z, Xianyou (2006) Preparation and Sinterability of Mn-Zn Ferrite Powders by Sol-Gel Method. J Rare Earths 24:5 4
16. Shahid M, Ramay A, Mahmood NS, Alzayed, Salem AS, Qaid (2017) Irshad Ali, Muhammad Tahir Farid, Structural and magnetic properties of praseodymium substituted strontium-based spinel ferrites. Journal of materials science: Materials in electronics 28:18656–18665
17. Jiahao Wang Y, Li R, Wu L, Xu Z, Zhang J, Feng J, Zhang L, Hou Y, Jiao, X-band shielding properties of Mg-9Li matrix composite containing $Ni_{0.4}Zn_{0.4}Co_{0.2}Fe_2O_4$ fabricated by multi-layer composite rolling, Journal of Alloys and Compounds, 843(202) 156053
18. Alina Manzoor MA, Khan MY, Khan MN, Akhtar A, Hussain (2018) Tuning magnetic and high frequency dielectric behavior in Li-Zn ferrites by Ho doping. Ceramics InternationalVolume 44(6):6321–6329
19. Bibi K, Ali I, Farid MT et al (2018) Electric and dielectric properties of Holmium substituted spinel ferrites. J Mater Sci: Mater Electron 29:3744–3750
20. REZLESCU N, REZLESCU E, POPA PD, C. DOROFTEI1, M. IGNAT1,COMPARATIVE STUDY BETWEEN CATALYST PROPERTIES OF SIMPLE SPINEL FERRITE POWDERS PREPARED BY SELF-COMBUSTION ROUTE, Romanian Reports in Physics, Vol. 65, No. 4, P. 1348–1356, 2013
21. Almessiere MA, Slimani Y, Rehman S, Khan FA, Gökçe Polat E, Sadaqat A, Shirsath SE, Baykal A (2020) Synthesis of Dy-Y co-substituted manganese–zinc spinel nanoferrites induced anti-bacterial and anti-cancer activities: Comparison between sonochemical and sol-gel auto-combustion methods, vol 116. C, Materials Science, p 111186
22. Mary George TL, Ajeesha A, Manikandan A, Anantharaman RS, Jansi E, Ranjith Kumar Y, Slimani MA, Almessiere A, Baykal (2021) Evaluation of Cu–MgFe2O4 spinel nanoparticles for photocatalytic and antimicrobial activates. Journal of Physics Chemistry of SolidsVolume 153:110010
23. Asiri S, Güner S, Korkmaz AD, Amir Md, Batoo KM, Almessiere MA, Gungunes H, Sözeri H, Baykal A (2018) Magneto-optical properties of BaCryFe12 − yO19 ($0.0 \leq y \leq 1.0$) hexaferrites. J Magn Magn Mater 451:463–472

24. Trukhanov SV, Trukhanov AV, Turchenko VA, Kostishyn VG, Panina LV, Kazakevich IS, Balagurov AM (2016) Structure and magnetic properties of BaFe11.9In0.1O19 hexaferrite in a wide temperature range. J Alloys Compd 689:383e393
25. Rhein F, Karmazin R, Krispin M, Reimann T, Gutfleisch O (2017) Enhancement of coercivity and saturation magnetization of Al3þ substituted M-type Sr-hexaferrites. J Alloys Compd 690:979e985
26. Janio Venturini, Rubia YS, Zampiva DH, Piva, Roger H, Piva, João Batista M. da Cunha and Carlos P. Bergmann Conductivity dynamics of metallic-to-insulator transition near room temperature in normal spinel $CoFe_2O_4$ nanoparticles,Journal of Material Chemistry C, 6 (2018) 4720–4726
27. Trukhanov SV, Trukhanov AV, Kostishyn VG, Panina LV, Trukhanov AV, Turchenko VA, Tishkevich DI, Trukhanova EL, Yakovenko OS, Matzui L (2017) Investigation of structure features and microwave absorption by doped barium hexaferrites. Dalton Trans 46:9010e9021
28. Zhang T, Peng X, Li J, Yang Y, Xu J, Wang P, Jin D, Jin H, Hong B, Wang X, Ge H (2017) Structural, magnetic and electromagnetic properties of SrFe12O19 ferrite with particles aligned in a magnetic field. J Alloys Compd 690:936e941
29. Tabatabaie F, Fathi MH, Saatchi A, Ghasemi A (2009) Microwave absorption properties of Mn- and Ti-doped strontium hexaferrite. J Alloys Compd 470:332e335
30. Yang Y, Wang F, Shao J, Huang D, He H, Trukhanov AV, Trukhanov SV (2018) Influence of Nd-NbZn co-substitution on structural, spectral and magnetic properties of M-type calcium-strontium hexaferrites Ca0.4Sr0.6-xNdxFe12.0-x(Nb0.5Zn0.5)xO19. J Alloys Compd 765:616e623
31. Almessiere MA, Slimani Y, Baykal A (2018) Impact of Nd-Zn co-substitution on microstructure and magnetic properties of SrFe12O19 nanohexaferrite. Ceram Int 45:963e969
32. Saba Yousaf I, Ahmad M, Kanwal T, Alshahrani, Hala HAlhashim, Kattan NA, Hafiz Muhammad Tahir Farid, Ahmer Riaz, Mehran T, Laref A, Structural and electrical properties of Ba-substituted spinel ferrites, Materials Science in Semiconductor Processing, 122 (2021) 105488
33. Shooshtary S, Yousefi VM, Amini MM, Shakeri AR, Bagherzad M (2019) Magnetic and microwave absorption properties of Cu/Zr doped M-type Ba/Sr hexaferrites prepared via sol-gel auto-combustion method. J Alloys Compd 773:1187e1194

Figures

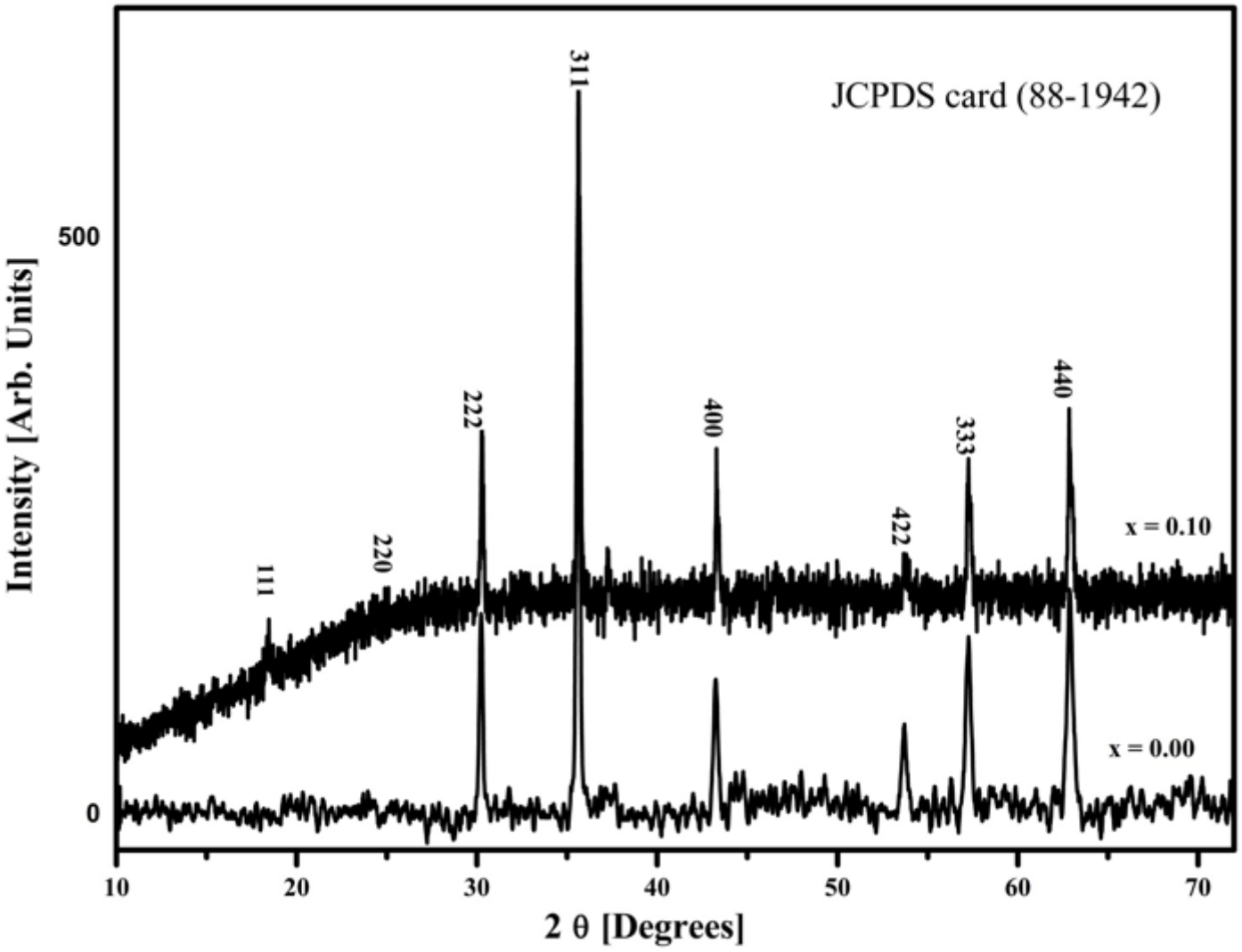

Figure 1

XRD patterns of spinel ferrites (x = 0.00 and 0.10).

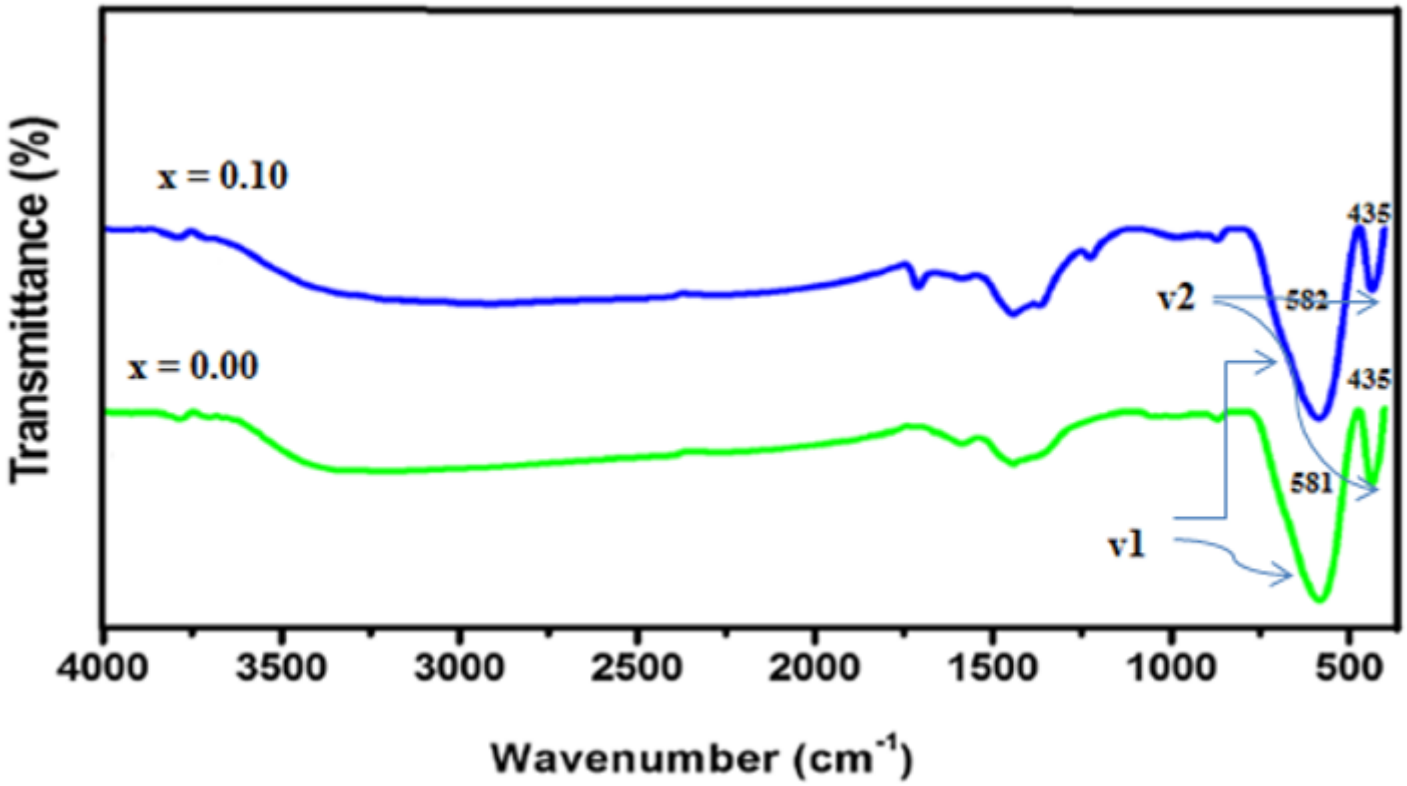

Figure 2

FTIR of spinel ferrites (x = 0.00 and 0.10).

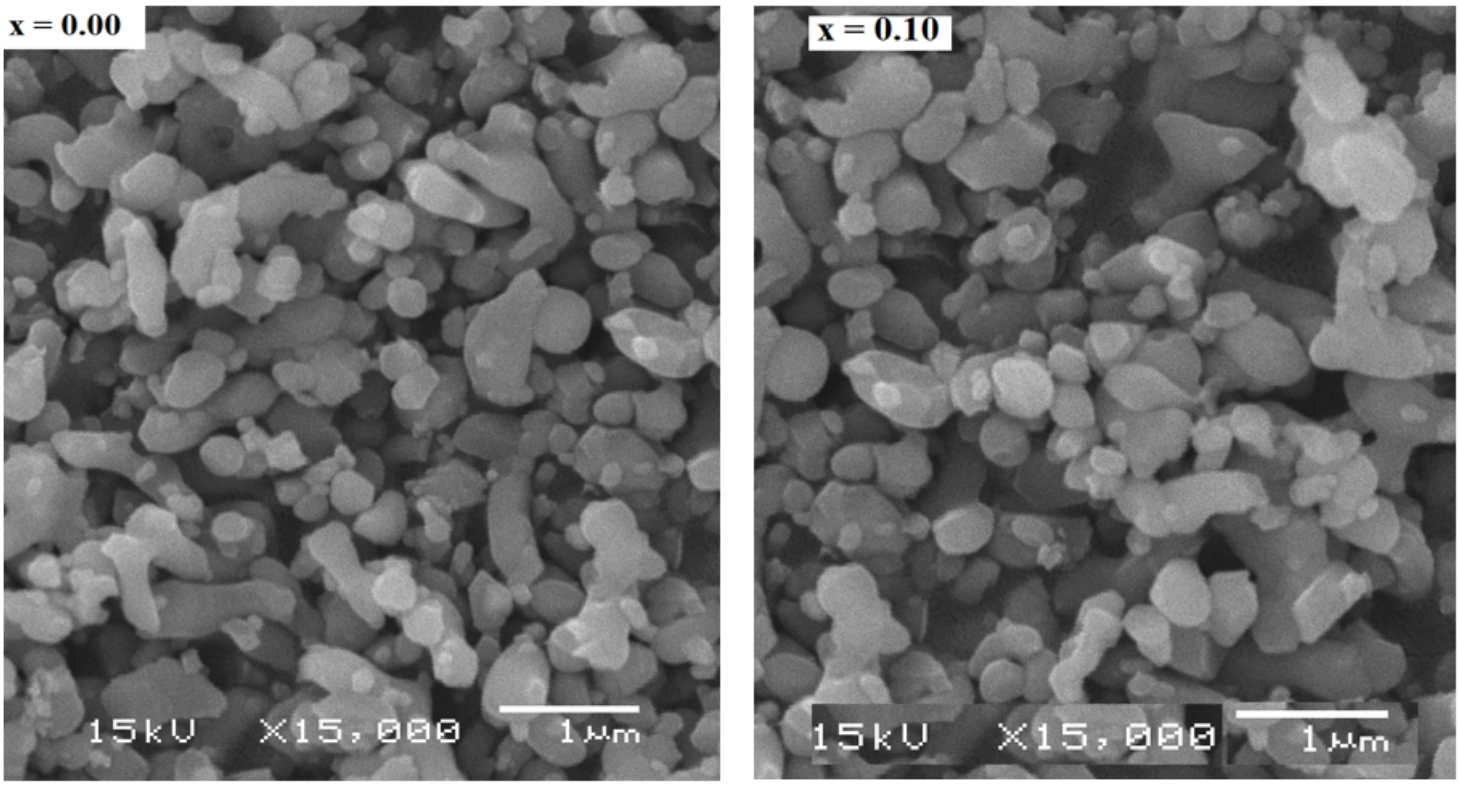

Figure 3

SEM of spinel ferrites.

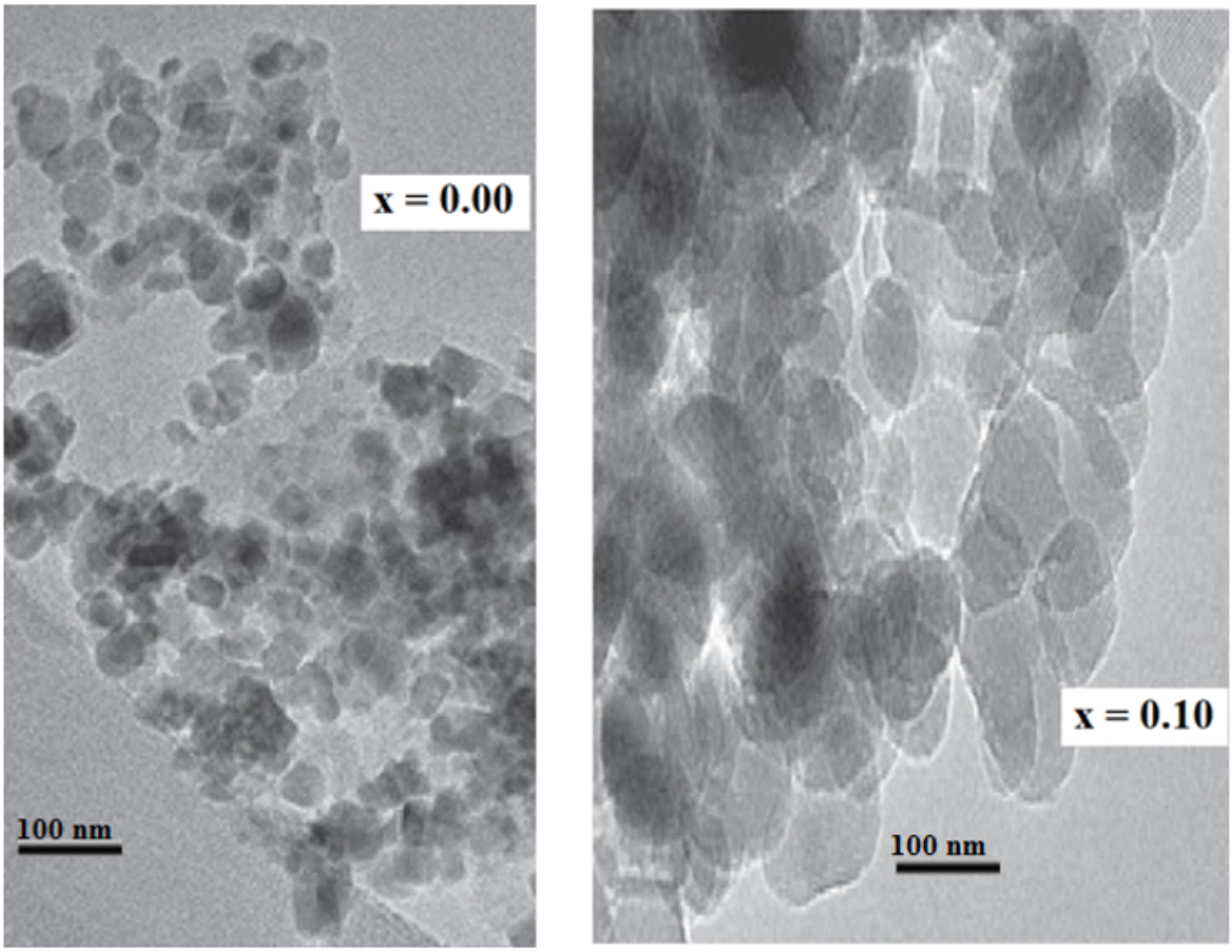

Figure 4

TEM of spinel ferrites.

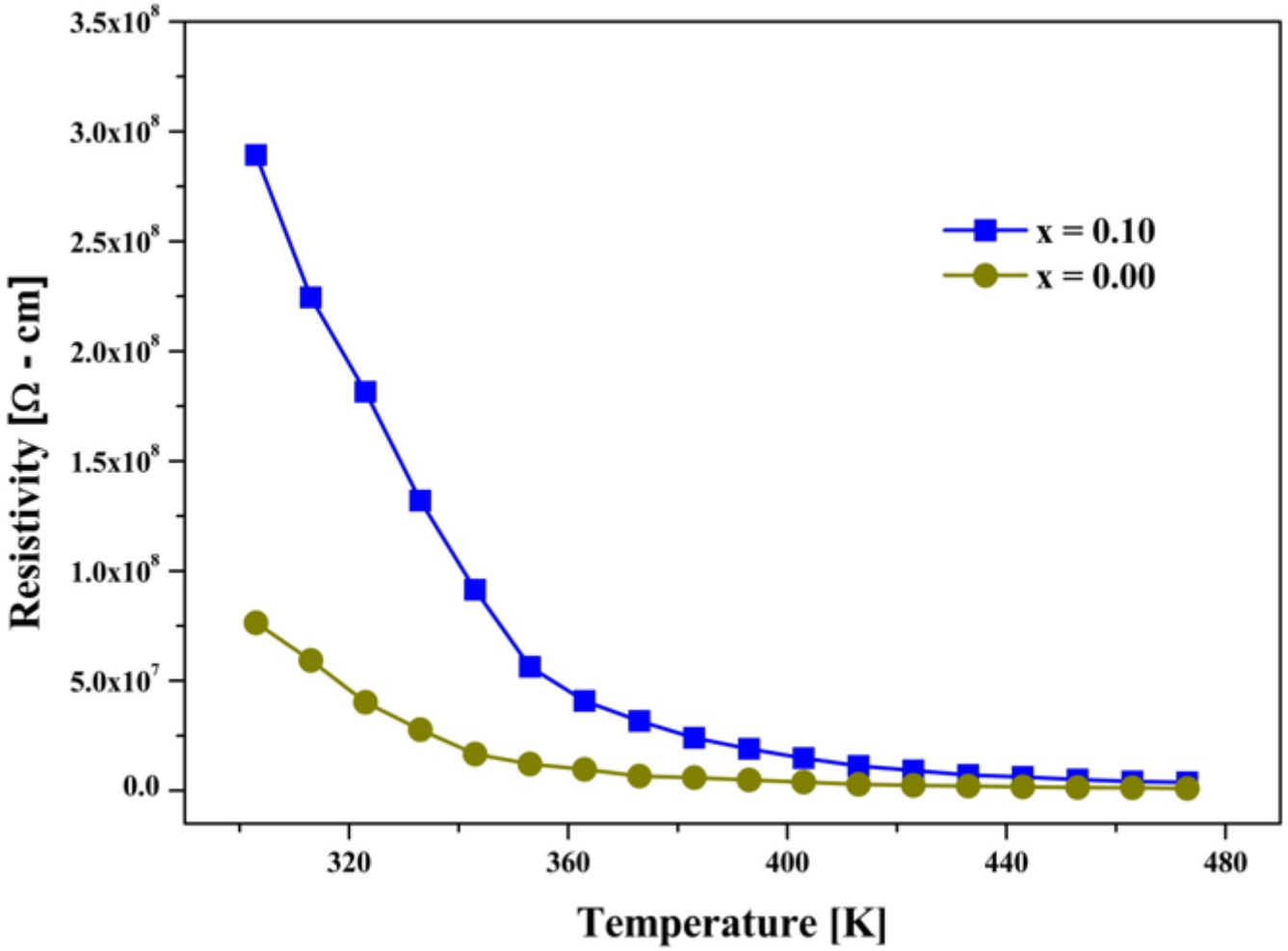

Figure 5

Variation of dc resistivity of spinel ferrite with temperature.

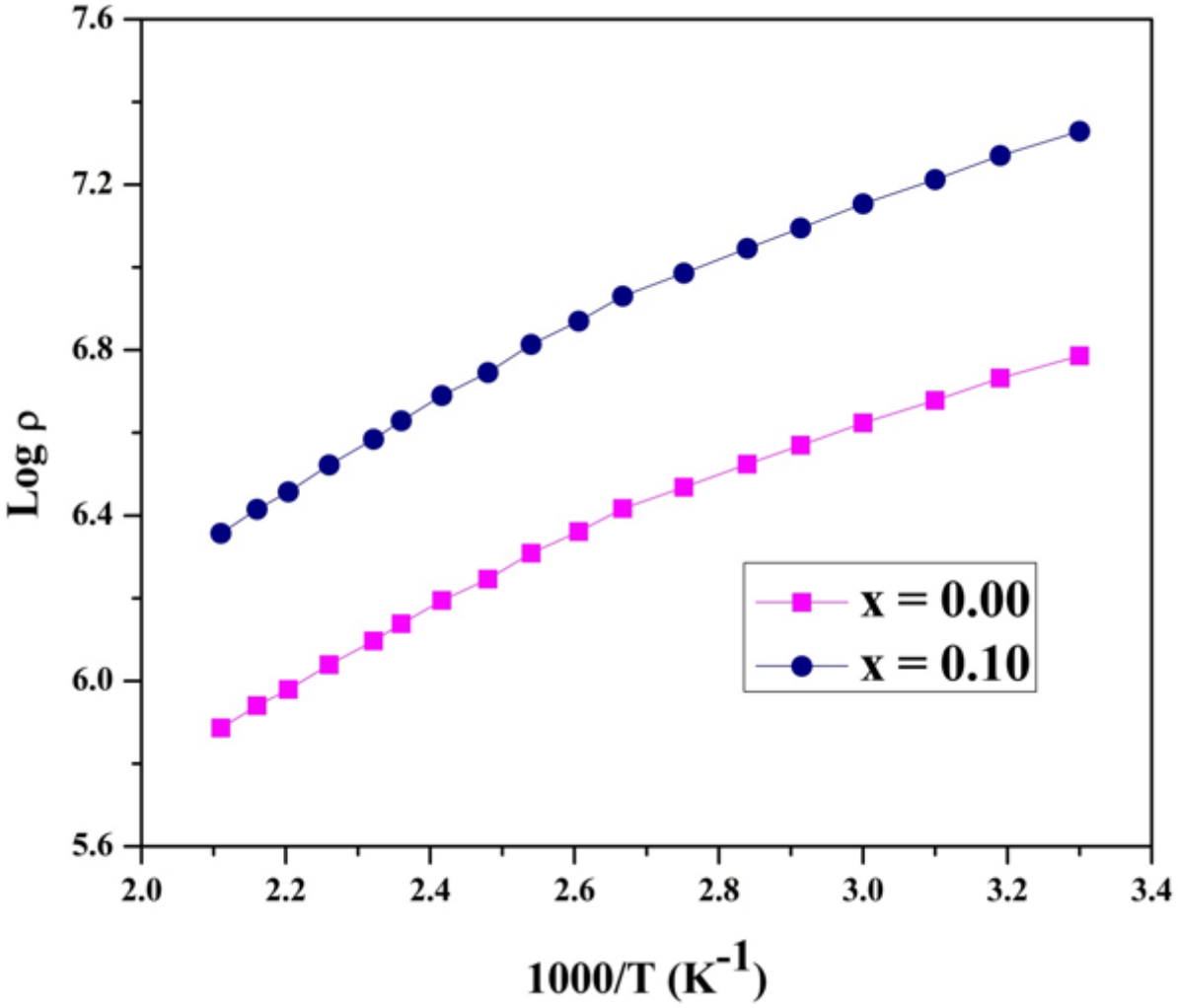

Figure 6

Variation of dc resistivity of spinel ferrite with 1000/T (K−1).

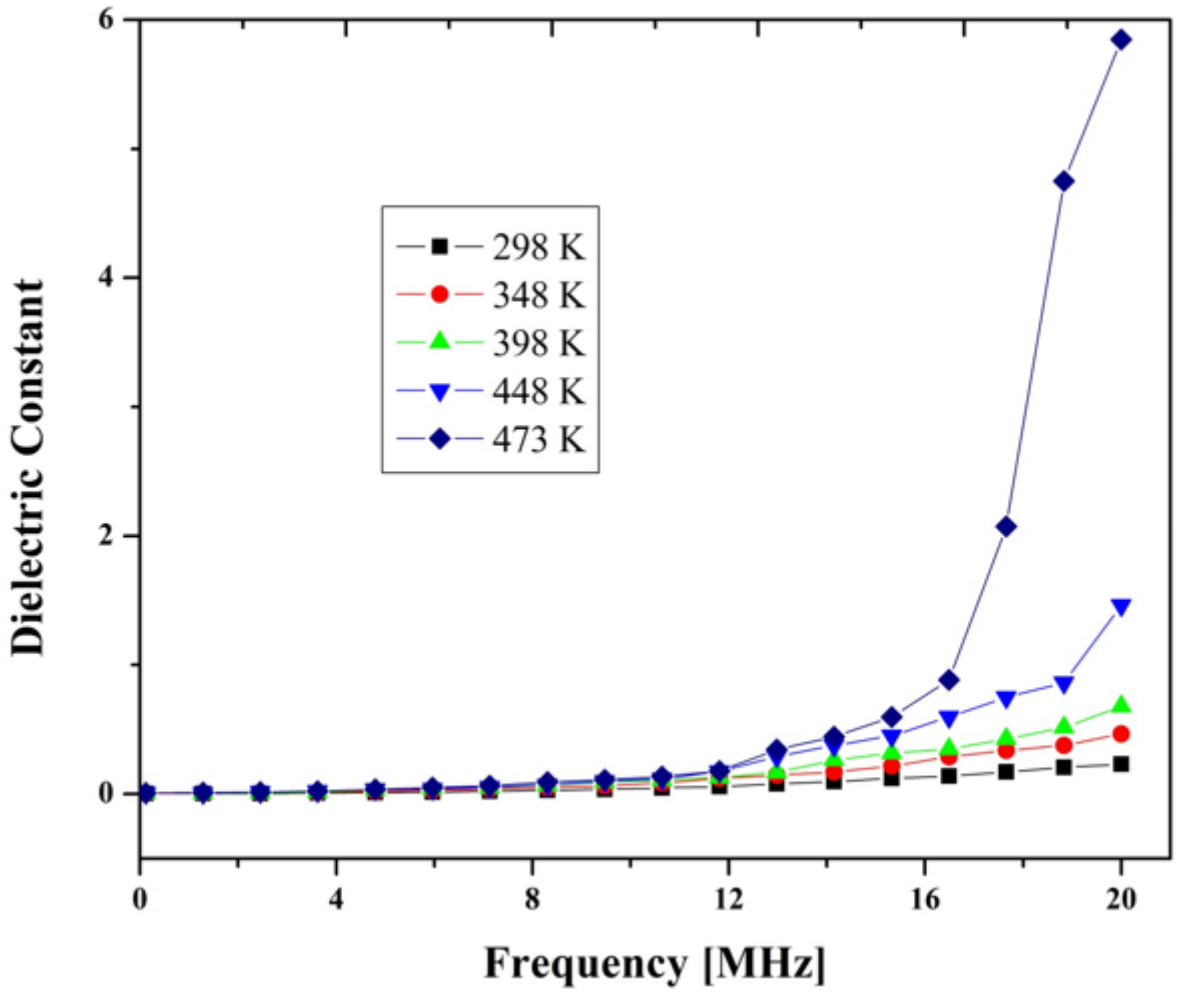

Figure 7

Variation of dielectric constant of spinel ferrite with frequency at different temperatures (x = 0.10).

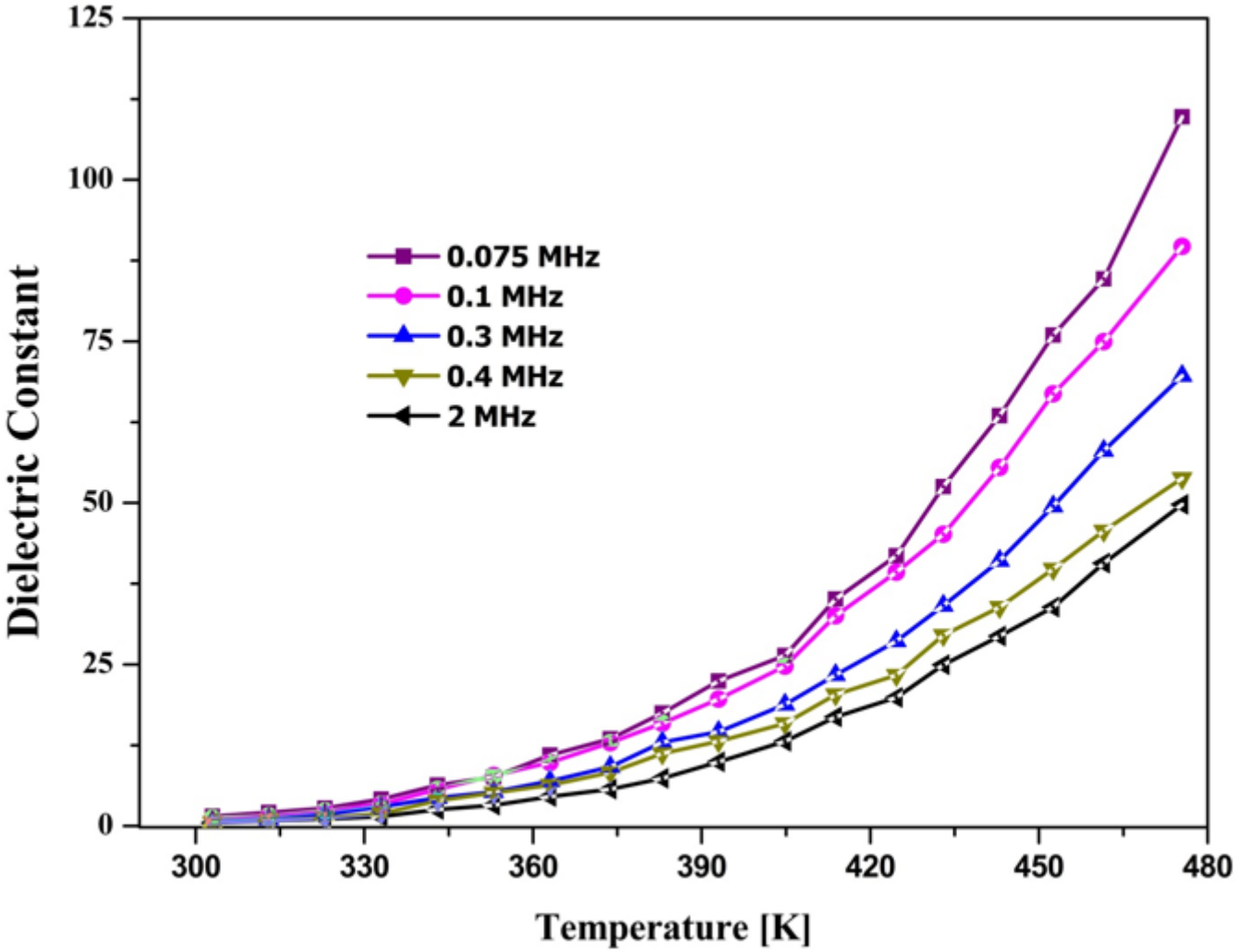

Figure 8

Variation of dielectric constant spinel ferrite with temperature at different frequencies (x = 0.1)..

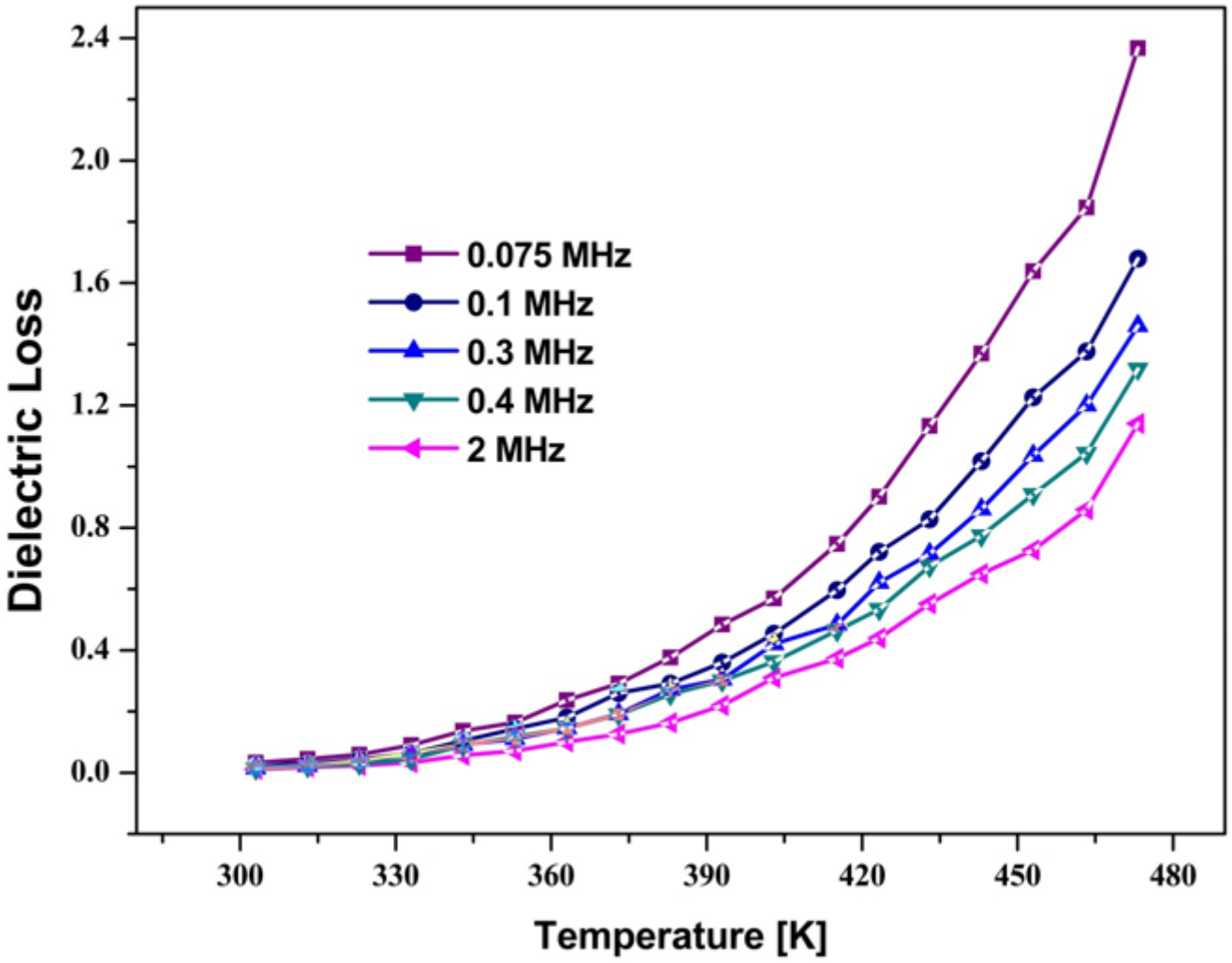

Figure 9

Variation of dielectric loss of spinel ferrite with frequency at different temperature (x = 0.1).

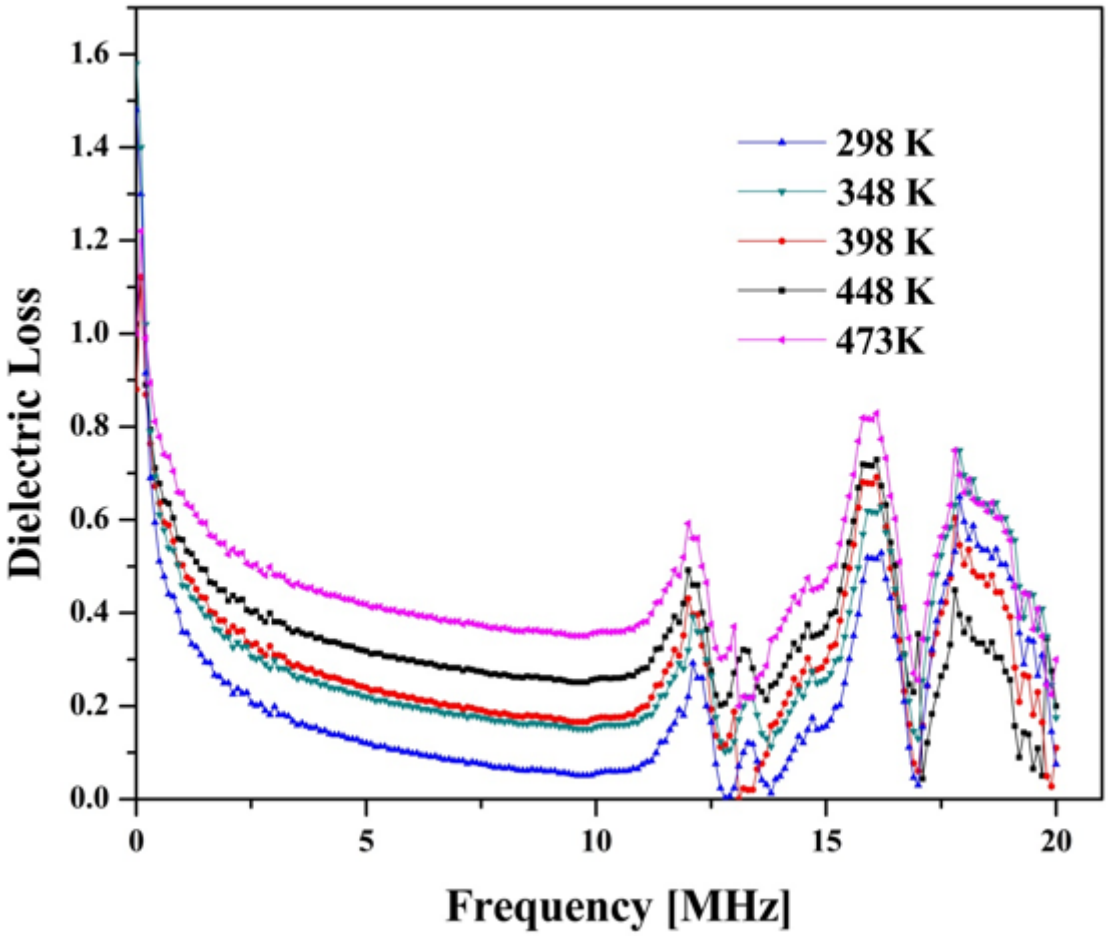

Figure 10

Variation of dielectric loss of spinel ferrite with temperature at different frequencies (x = 0.1).

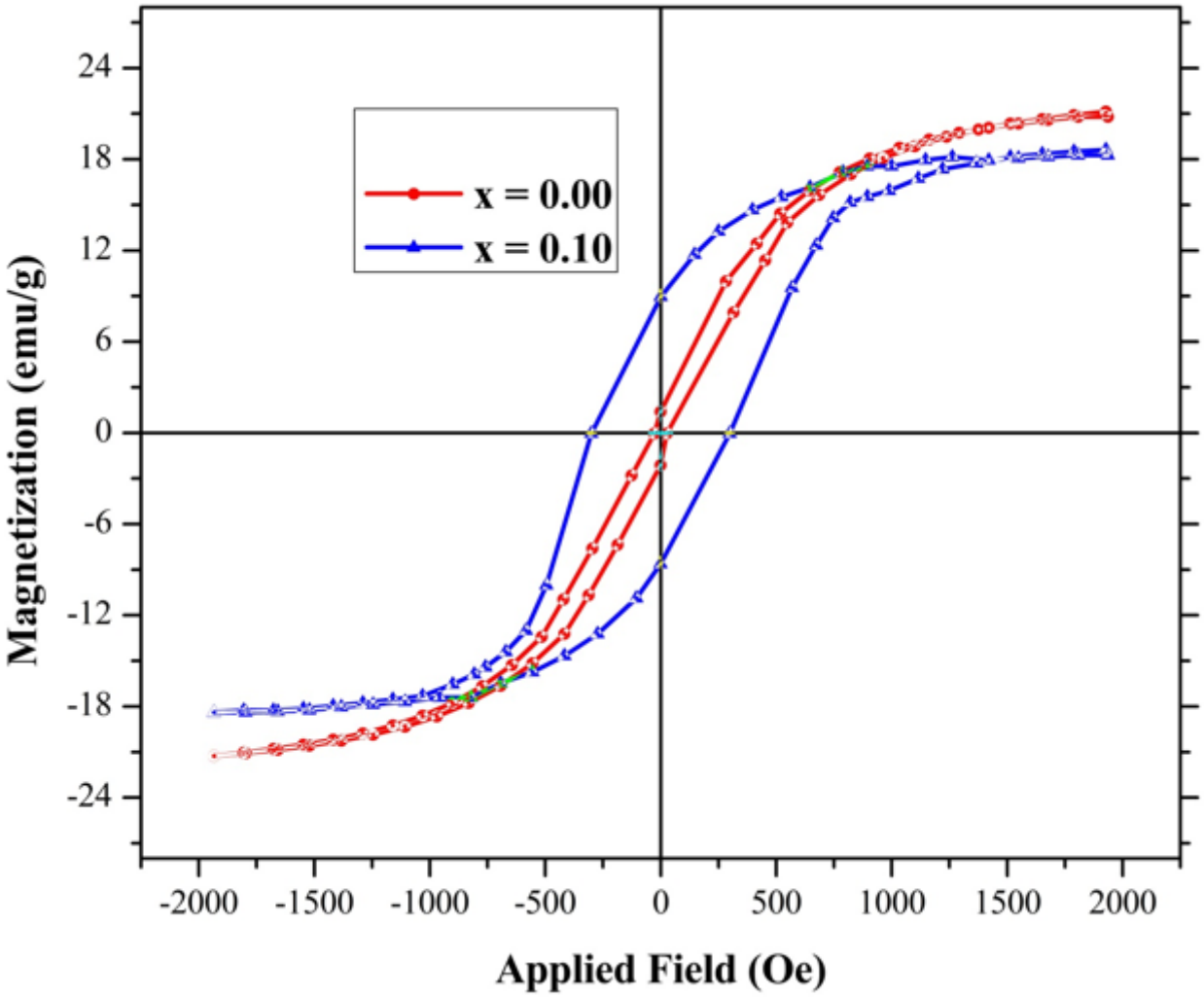

Figure 11

M-H loops of spinel ferrite.